Normal-state bubbles and lamellae in type-I superconductors

A. Cēbers,[1] C. Gourdon,[2,*] V. Jeudy,[2] and T. Okada[2,3]
[1]*Institute of Physics, University of Latvia, Salaspils-1, LV-2169, Latvia*
[2]*Institut des Nanosciences de Paris, CNRS UMR 7588, Universités Paris 6 et 7, Campus Boucicaut, 140 rue de Lourmel, 75015 Paris, France*
[3]*Itoh Laboratory, Division of Materials Physics, School of Engineering Science, Osaka University, 1-3 Machikaneyama-cho, Toyonaka-shi, Osaka 560-8531, Japan*
(Received 22 July 2004; revised manuscript received 28 January 2005; published 8 July 2005)

We report an extensive study of the formation of normal-state domains in type-I superconductors. Domain patterns are first considered theoretically. The magnetic interaction between domains is described in the framework of the "current-loop" model: the intermediate state is modeled by a set of loops of screening current encircling the domains and interacting as in the free space. This system is shown to be formally equivalent to a set of uniformly magnetized domains. An extension of the current-loop model is proposed to take into account the constraint of the magnetic shielding by the superconducting regions. We determine the free energy of a hexagonal array of cylindrical domains (bubbles) and of a lattice of infinitely long and parallel stripes. The equilibrium values of both the volume fraction of the normal phase and the domain size are calculated as functions of the magnetic field. A bubble-to-stripe transition is predicted to occur for a volume fraction of the normal phase about 0.3. Experimentally, normal-state domains are studied with the high-resolution magneto-optical imaging technique. The observed patterns consist in coexisting bubbles and disordered labyrinthine lamellae structures. We show evidence of the contribution of pinning on the position of domain interfaces. The average width of the lamellae is then analyzed as a function of the applied magnetic field and found to increase in good agreement with the predictions. In contrast, the average diameter of bubbles remains constant: it is almost independent of the magnetic interaction between domains. A very good agreement, over three decades of the magnetic Bond number, is found with the equilibrium diameter of an isolated bubble. The proposed constrained current-loop model is shown to provide significantly more accurate predictions than the current-loop model, in particular for small magnetic Bond numbers. Additionally, increasing the volume fraction of the normal phase results in a bubble-to-lamella transition, as predicted theoretically.

DOI: 10.1103/PhysRevB.72.014513 PACS number(s): 74.25.Ha, 75.70.Kw, 05.65.+b

I. INTRODUCTION

Self-organization in domains is observed in many quasi-two-dimensional systems where two phases coexist: polarized Langmuir monolayers confined at air-water interfaces,[1,2] ferrofluids,[3–8] ferro- and ferrimagnetic thin films,[9,10] the intermediate state (IS) in type-I superconductors,[11–13] adsorbates on a metal substrate,[14] and in different nonequilibrium systems, for example, those described by reaction-diffusion equations.[15,16] Pattern formation essentially results from the competition between long-range (electrostatic, magnetostatic, or elastic) forces between domains and short-range forces described by an interfacial tension between the two phases. A review of these pattern formation processes is given in Ref. 17. The static and dynamic properties of those structures are actively studied theoretically.[4,18,19]

IS patterns in type-I superconductors consist of fully diamagnetic, superconducting (SC) domains coexisting with normal-state (NS), flux-bearing domains of complex shape.[13] They are observed in samples with large demagnetizing factor such as thin films placed in a perpendicular magnetic field. At very low applied field the sample is in the Meissner state: the magnetic flux is totally expelled. Due to the demagnetizing factor, the local magnetic field on the sharp edges of the sample is larger than the applied field. The magnetic flux starts to penetrate into the sample when this local field reaches the thermodynamic critical field. The sample exhibits coexisting NS and SC regions up to the complete transition to the NS. The most frequently encountered structures consist of cylindrically shaped domains (bubbles or flux tubes) and of branched and intricate fingered domains (lamellae). The lamellar structure has been extensively studied since the first calculation of the free energy of a lattice of infinitely long and parallel stripes by Landau.[20] This two-dimensional problem was solved by the conformal mapping technique. The field-dependent predicted and measured periods were found to be in good agreement,[21,22] thus suggesting that lamellar structures correspond to a quasiground state. In contrast, little is known about the static properties of bubble patterns. The main difficulty for modeling the magnetic interaction of a hexagonal array of cylindrical domains originates in the three-dimensional nature of the problem. A previous calculation uses an approximate expression of the magnetic energy[23] and leads to predicted field-dependent bubble spacings different from the measured ones.[22–25] As a result, it is not established whether the observed bubble patterns also correspond to quasiground states. Moreover, the origin of the coexistence between bubbles and lamellar observed experimentally is not well understood. In particular, whether bubble or lamellae structures constitute the ground state of the IS remains an open theoretical question.

A promising approach to the pattern formation in type-I superconductors arises due to the current-loop (CL) model. This model, proposed in Refs. 19 and 26, is adapted from

formalisms developed for pattern formation in thin ferromagnetic films and ferrofluids.[3,9] It is based on the analogy which exists between the interaction of the superconducting currents screening the magnetic field in the normal phase and interaction between domains in thin films of ferromagnetics or ferrofluids. This analogy comes from magnetostatics when the magnetic fields created by a solenoid of finite height and a magnetized body with the same shape are considered. Since in type-I superconductors the penetration length λ is less than the coherence length ξ determining the thickness of the transition layer between the SC and normal phases and ξ usually is much smaller than other characteristic lengths in the system[27] (distance between the domains, thickness of the film) then, in the sharp interface limit, it is possible to consider the phase interface as a current loop of finite height. The current loops are then assumed to interact as in free space. For a lattice of stripes, predicted field-dependent periods are close to those calculated by Landau and in good agreement with the experimental findings.[28] This suggests that the CL model reasonably well describes the magnetic interactions between domains. Moreover, as the CL model is formulated for arbitrary domain shape, it can be applied to the bubble pattern.[29] It should also allow us to determine the ground state of the IS bubble or stripe phase as a function of the volume fraction of the normal phase, which is impossible to solve by the existing approaches, and to compare it to the structures experimentally observed. However, the CL model does not take into account a specific feature of superconductors: the existence of screening currents on the top and bottom surfaces of the films. The importance of this effect on the domain structure of the IS state and on the period and size of the IS patterns needs to be considered. We propose to modify the CL model in order to include this screening effect.

IS models assume that the system reaches equilibrium conditions for any variation of the external parameters. However, it is well known experimentally that the formation of the IS depends on the magnetic history of the samples due to irreversible processes. An important issue is to determine how far from equilibrium the system is brought by these processes. First, domains can be pinned by defects. Pinning may induce disorder in the IS structures and limit the free motion and the growth of domains. Second, the variation of the volume fraction of the NS phase can only result from penetration of magnetic flux on the edges of samples.[30] This penetration is known to be irreversible and controlled by an energy barrier of geometrical nature.[31,32] The mechanism of flux penetration probably drives the early stage of the formation of domains. The respective contributions of the nucleation of flux domains on the edges of the sample and of the competition between short-range and long-range forces in the observed patterns need to be studied. Moreover, in contrast to other physical systems that exhibit self-organized structures, the growth of NS domains with an applied magnetic field may depend on whether the NS domains are isolated or not in the SC phase.[33] This consequence of the specific properties of the SC phase has not been thoroughly investigated yet. In the experimental part of this paper, we analyze the respective contributions of the sources of irreversibility mentioned above and of the competition between short-range and long-range interactions in the formation of domains.

The outline of this paper is as follows. Sections II and III are devoted to theory. In Sec. II we analyze the CL model and the approximations involved. Interface dynamics is discussed. As an improvement of the CL model we propose the constrained current-loop (CCL) model in order to account for the magnetic screening by the superconducting surface currents. We discuss its validity for thin films. In Sec. III the energies of the periodic stripe phase and bubble hexagonal phase are calculated. We obtain the dependence of the density of the normal phase and of the size of domains on the applied magnetic field. Section IV describes the experimental setup and presents qualitative features of IS patterns. The importance of pinning is investigated. We also discuss the validity of the usual approximation that consists in taking the magnetic field in NS domains equal to the critical field. Section V is devoted to the study of the growth of lamellae. The field dependence of the lamellar width is compared to theoretical predictions. Section VI presents a very important result of this paper: we show that the mean diameter of bubbles is independent of the magnetic interaction between them. An interpretation that takes into account the specific properties of the SC phase is proposed. The CCL model is found to provide a much better agreement with experimental results than the CL model. Section VII presents results on the transition from flux tubes to flux lamellae. A summary of the results and perspectives for future studies are given in the conclusion.

II. CURRENT-LOOP MODEL

A. General relations

To calculate the magnetic field energy of the intermediate state $(1/8\pi)\int \vec{h}^2 dV$, accounting for the Meissner effect, we take $\vec{h}_s=0$ and $\vec{h}_n=\vec{H}_n$ (the indices s and n denote the superconducting and normal phases, respectively). In the sharp interface limit the jump of the magnetic field strength on the phase boundary is

$$\Delta\vec{h} = -\vec{H}_n.$$

The magnetic field strength $\vec{h}$ can be written as a sum of the magnetic field created by the external coils $\vec{H}_0$ and the magnetic field $\vec{H}$ created by the superconducting currents: $\vec{h}=\vec{H}_0+\vec{H}$. As a result the expression for the magnetic energy is

$$E_m = \frac{1}{8\pi}\int \vec{h}^2 dV = \frac{1}{8\pi}\int \vec{H}_0^2 dV + \frac{1}{4\pi}\int \vec{H}_0\vec{H}\, dV + \frac{1}{8\pi}\int \vec{H}^2 dV. \quad (1)$$

The magnetic field of the intermediate state created by the superconducting currents on the border of film is $\vec{H}_\infty$ and that of the superconducting currents around the domains of the normal phase $\vec{H}'$. Thus $\vec{H}=\vec{H}_\infty+\vec{H}'$. The magnetic energy

terms in relation (1) are transformed as follows ($\vec{h}=\mathrm{rot}\,\vec{A}$):

$$\frac{1}{4\pi}\int \vec{H}_0\vec{H}\,dV = \frac{1}{4\pi}\int (\vec{h}-\vec{H})\vec{H}\,dV = \frac{1}{c}\int \vec{A}\vec{j}_s dV - \frac{1}{4\pi}\int \vec{H}^2 dV. \quad (2)$$

In the sharp interface limit, since $\lambda < \xi$, the first term in relation (2) reads ($\vec{i}_s$ is the surface density of the superconducting currents, and summation over i means the sum with respect to all domains of the normal phase)

$$\frac{1}{c}\int_{S_\infty} \vec{A}\vec{i}_s dS + \frac{1}{c}\sum_i \int_{S_i} \vec{A}\vec{i}_s dS. \quad (3)$$

The integral in the first term of relation (3) is around the border of the superconductor film, but the second term takes into account all inclusions of the normal phase. The boundary condition for the surface current density on the interface of the domain of the normal phase is

$$\vec{i}_s = -\frac{c}{4\pi}[\vec{n}\times\vec{h}_n]. \quad (4)$$

Here $\vec{n}$ is the external normal to the surface of the domain, but $\vec{h}_n$ is the magnetic field strength in the normal phase. In the mean-field approximation $\int_{L_i}\vec{A}\,d\vec{l}=\Phi_n=H_nS_i$, the second term in relation (3) can be written as

$$\frac{1}{c}\sum_i \int_{S_i} \vec{A}\vec{i}_s dS = \frac{1}{4\pi}\sum_i \int_{L_i}\int \vec{A}\,d\vec{l}\,H_n dz = \sum_i \frac{1}{4\pi} S_i H_n^2 d = \frac{1}{4\pi} H_n^2 \rho_n V.$$

Here $H_n\vec{e}_z$ is the mean value of $\vec{h}_n$ across the film with thickness d and $\rho_n=S_n/S$ is the density of the normal phase.

The expression for the magnetic energy of the superconducting currents $(1/8\pi)\int \vec{H}^2 dV$ can be transformed as follows:

$$\frac{1}{8\pi}\int \vec{H}^2 dV = \frac{1}{8\pi}\int \vec{H}'^2 + \frac{1}{4\pi}\int \vec{H}_\infty \vec{H}'\,dV + \frac{1}{8\pi}\int \vec{H}_\infty^2 dV. \quad (5)$$

The second term in the relation (5) can be transformed as follows:

$$\frac{1}{4\pi}\int \vec{H}_\infty\vec{H}'\,dV = \frac{1}{c}\int_{S_\infty} \vec{A}'\vec{i}_s dS.$$

Finally for the magnetic energy of the intermediate state we have

$$\frac{1}{8\pi}\int \vec{h}^2 dV = \frac{1}{8\pi}\int \vec{H}_0^2 dV - \frac{1}{8\pi}\int \vec{H}_\infty^2 dV + \frac{1}{c}\int_{S_\infty} (\vec{A}_0+\vec{A}_\infty)\vec{i}_s dS + V\frac{1}{4\pi}H_n^2\rho_n - \frac{1}{8\pi}\int \vec{H}'^2 dV. \quad (6)$$

The last two terms in relation (6) are relevant for the description of the transitions between the different patterns of the intermediate state. We introduce the notation

$$E_m = V\frac{1}{4\pi}H_n^2\rho_n - \frac{1}{8\pi}\int \vec{H}'^2 dV.$$

E_m can be put in an equivalent form using the analogy which exists between the magnetic field created by a solenoid with finite height and a magnetized body with the shape of a solenoid. The convenience of this transformation is in the fact that it allows us to obtain in explicit form the terms determining the density of the normal phase in the case of thick films when the magnetic interactions between the domains of normal phase are not important. To do this we put

$$\vec{H}' = H_n\vec{e}_z\Theta(V_n) + \tilde{\vec{H}}. \quad (7)$$

Here the Heaviside function Θ is equal to 1 in the domains of the normal phase and to zero outside. H_n according to relation (4) is determined by the superconducting currents circulating on the interface of the normal phase,

$$H_n\vec{e}_z = \frac{4\pi}{c}[\vec{n}\times\vec{i}_s].$$

Due to Eq. (7) $\tilde{\vec{H}}$ is continuous on the part of the interface normal to the boundaries of the film and can be expressed as the gradient of a potential ($\tilde{\vec{H}}=\nabla\psi$). The normal component of $\tilde{\vec{H}}$ on the part of the boundary of the film belonging to the normal phase is discontinuous. Its jump there is equal to

$$\vec{e}_z(\tilde{\vec{H}}^e - \tilde{\vec{H}}^i) = H_n. \quad (8)$$

Thus

$$\frac{1}{8\pi}\int \vec{H}'^2 dV = \frac{H_n^2 V_n}{8\pi} + \frac{1}{4\pi}\int_{V_n} \tilde{H}_z^i H_n dV + \frac{1}{8\pi}\int \tilde{\vec{H}}^2 dV. \quad (9)$$

The second term in relation (9) is transformed as follows:

$$\frac{1}{4\pi}\int_{V_n} \tilde{H}_z^i H_n dV = \frac{1}{4\pi}\int \psi^i\left(\frac{\partial\psi^e}{\partial n} - \frac{\partial\psi^i}{\partial n}\right)dS = -\frac{1}{4\pi}\int \tilde{\vec{H}}^2 dV.$$

Thus for E_m we have

$$E_m = V\frac{1}{8\pi}H_n^2\rho_n + \frac{1}{8\pi}\int \tilde{\vec{H}}^2 dV.$$

The first term in this relation corresponds to the magnetic field energy of the normal phase of an infinitely thick

sample; the second describes the demagnetizing field energy correction due to the finite thickness of the sample. According to the relation (8) ψ can be expressed by the sum of two single-layer potentials created by surface charges with densities $\mp(1/4\pi)H_n$ at $z=d$ and 0, respectively,

$$\psi = -\frac{H_n}{4\pi}\int \frac{dS'}{\sqrt{(\vec{\rho}-\vec{\rho}')^2+(z-d)^2}} + \frac{H_n}{4\pi}\int \frac{dS'}{\sqrt{(\vec{\rho}-\vec{\rho}')^2+z^2}}.$$

Due to the symmetry, one has $\psi_+ = \psi(z=d) = -\psi(z=0) = -\psi_-$. As a result

$$\frac{1}{8\pi}\int \tilde{\vec{H}}^2 dV = \frac{1}{8\pi}\int \psi^j\left(\frac{\partial\psi^j}{\partial n} - \frac{\partial\psi^e}{\partial n}\right)dS = -M\int \psi_+ dS; \tag{10}$$

here

$$\psi_+(\vec{\rho}) = -M\int J(\vec{\rho}-\vec{\rho}',d)dS' = -\int M\,dS'\left(\frac{1}{\sqrt{(\vec{\rho}-\vec{\rho}')^2}} - \frac{1}{\sqrt{(\vec{\rho}-\vec{\rho}')^2+d^2}}\right) \tag{11}$$

where $M=(1/4\pi)H_n$ is the effective magnetization of the normal phase. The first and second terms in the expression for J correspond to the interaction of fictitious magnetic charges located on the same and on the opposite side of the sample. Depending on the way they are taken into account different models (CL and CCL) are obtained. The full free energy of the problem accounting for the condensation energy of the superconducting phase $(1/8\pi)H_c^2$ and the surface energy of the interfaces between the normal and superconducting phases [the surface tension σ of the interface between the normal and superconducting phases is usually represented as $(H_c^2/8\pi)\Delta$, introducing the wall energy parameter Δ] reads

$$F = F_{supra} + V\left(\frac{1}{8\pi}H_c^2\rho_n + \frac{1}{8\pi}H_n^2\rho_n\right) + \sum_i \sigma d\int_{L_i} dl + \frac{1}{8\pi}\int \tilde{\vec{H}}^2 dV. \tag{12}$$

The term in parentheses contains the condensation energy and the bulk magnetic energy of a uniformly magnetized sample; the next term is the surface energy. The last term describes the correction due to the finite thickness of the sample.

B. Constrained current-loop model

The representation of the magnetic field created by the superconducting currents on the boundaries of the domains of the normal phase given by Eqs. (7) and (11) allows us to account for screening superconducting currents on the top and bottom surfaces of the film, at least for thin samples, which are neglected in the existing version of the CL model[19,26] (see discussion on this in Refs. 34 and 35). Here we give the argument that accounting for the screening superconducting surface currents corresponds to the kernel J in relation (11) at $d\to\infty$. Indeed, considering the domain of the normal phase the boundary conditions on its top and bottom surfaces are

$$\frac{\partial\psi^e}{\partial z} - \frac{\partial\psi^j}{\partial z} = H_n. \tag{13}$$

On the top and bottom surfaces of the surrounding superconducting regions we have

$$\frac{\partial\psi^e}{\partial z} = 0.$$

For a thin film of superconductor the mixed boundary value problem arises for the harmonic magnetostatic potential ψ satisfying the condition $\psi(\vec{\rho},z) = -\psi(\vec{\rho},-z)$, whose solution can be obtained from the integral equation[36] ($\vec{\rho}\in S_n$)

$$H_n = \int_{S_n} K(\vec{\rho},\vec{\rho}')\psi(\vec{\rho}',0^+)dS_{\vec{\rho}} \tag{14}$$

The expression for the kernel $K(\vec{\rho},\vec{\rho}')$ follows from the Greens function of the Dirichlet problem for the semispace. The solution of Eq. (14) is known for the circular shape of the domain[36]

$$\psi(\vec{\rho},0^+) = -\frac{2H_n}{\pi}\sqrt{R^2-r^2}.$$

This allows us to calculate the last term in relation (12):

$$\frac{1}{8\pi}\int \tilde{\vec{H}}^2 dV = \frac{1}{8\pi}\int \psi\frac{\partial\psi}{\partial n}dS = \frac{H_n^2R^3}{3\pi}. \tag{15}$$

This is just the expression of the magnetic energy of the circular domain of the normal phase obtained in the limit $d\to\infty$ from the general relations for the hexagonal lattice of the domains of normal phase given in Appendix B. In this limit for small volume fractions of the normal phase when the interactions between different domains can be neglected we have

$$E_m = N\frac{H_n^2R^3}{3\pi} + V\frac{1}{8\pi}H_n^2\rho_n.$$

This corresponds to the magnetic energy with the correction term given by the relation (15). The last relation when put in an equivalent form

$$E_m = \frac{N\pi R^2 dH_n^2}{8\pi}\left(1+\frac{8R}{3\pi d}\right)$$

coincides with the one given by the correction to the self-induction of a solenoid L of finite length derived in Ref. 33 for small R/d,

$$L = L_\infty\left(1-\frac{8R}{3\pi d}\right).$$

Our argument shows that due to the screening superconducting surface currents this correction term works even for

small d when the approximate expression for the correction term should not be valid anymore. Moreover, as illustrated below in the limit of small volume fractions of the domains of the normal phase the minimization of the energy of the hexagonal phase with respect to the period of the structure is equivalent to the minimization of the energy per unit area of the domain with respect to its radius.[29] Accounting for the surface energy of the domain $2\pi\sigma Rd$, the energy per unit area of the domain is

$$\frac{H_n^2 R}{3\pi^2} + \frac{2\sigma d}{R}.$$

Taking into account that $H_n = H_c$ for small volume fractions of the normal phase, minimization with respect to R leads to

$$\frac{2R}{d} = \sqrt{\frac{3}{2\mathrm{Bm}}}. \tag{16}$$

Here the magnetic Bond number $\mathrm{Bm} = M_c^2 d/\sigma = d/2\pi\Delta(M_c = H_c/4\pi)$ characterizing the ratio of the magnetic and surface forces is introduced. The relation (16), as shown in Sec. VI, is in very good agreement with the existing experimental data. It is important that relation (16) works even for small thicknesses of the film when the asymptotics $d \to \infty$ of the CL model is not supposed to be valid. According to the above discussion we could expect such behavior since the CL model in the limit $d \to \infty$ takes into account screening superconducting currents on the top and bottom surfaces of the film. We name this limit of current-loop model the constrained current-loop model.

The validity of the CCL model is further demonstrated by considering the instabilities of the stripe pattern. An analysis of the serpentine instability of the stripe phase of the intermediate state taking into account the screening superconducting currents was recently carried out in Ref. 28. The general expression for the magnetic energy of slightly buckled periodic system of stripes in the frame of CL model is derived in Ref. 37. The magnetic energy per stripe e_m in the buckled state can be expressed as follows:[37]

$$e_m = \frac{1}{2\pi} \int dq |\zeta(q)|^2 [F(q) - F(0)]. \tag{17}$$

Here (a is the period of the structure, $2w$ is the stripe width)

$$F(q) = \sum_{k=1}^{\infty} \frac{16\pi M^2}{a\sqrt{(2\pi k/a)^2 + q^2}} \times [1 - \exp(-\sqrt{(2\pi k/a)^2 + q^2} d)] \sin^2\left(\frac{2\pi w k}{a}\right). \tag{18}$$

$\zeta(y) = (1/2\pi) \int \zeta(q) \exp(iqy) dq$ is periodic along the y axis stripe boundary displacement. Transforming the expression of the energy variation to discrete Fourier modes considered in Ref. 28, $\zeta_n = (1/L_y)\zeta(q)$, $q = 2\pi p/L_y$, where L_y is the size of the system in the y axis direction in the limit $d \to \infty$ and $\zeta = \epsilon \cos(\nu_0 y)$, the relation (17) for the variation of the magnetic energy per unit surface area gives

$$\frac{H_c^2}{8\pi} \sum_{k=1}^{\infty} \frac{\sin^2(2\pi w k/a)}{4\pi^2} \left(-\frac{1}{k 2\pi/a} + \frac{1}{\sqrt{[(2\pi k)/a]^2 + \nu_0^2}} \right). \tag{19}$$

This is just the relation derived in Ref. 28 taking into account screening superconducting currents. On the basis of the relation (19) the experimentally observed development of the serpentine instability has been described. This illustrates the usefulness of the CCL model for the description of the serpentine instability of the intermediate state. It should be remarked that on transformation of the relation (17)–(19) also a multiplier of 1/2 has been accounted for since in Ref. 28 only one interface of the film is considered.

The above discussion illustrates the versatility of the approach connected with the consideration of the analogy between a magnetized body and a solenoid of finite height with the same shape. This allows us in a simple way to obtain the expressions for the magnetic energy of thin samples taking into account the screening by the superconducting currents.

On the basis of the general expression for the energy of the intermediate state (12) different problems can be considered. One of them is the long-standing problem of the transition between hexagonal and stripe phases considered already in Ref. 23. Nevertheless the approximate expressions for the energies of the hexagonal and the stripe phases given in Ref. 23 show that they are close but do not indicate a hexagon-stripe transition, which is observed in experiments (see Ref. 29 and below). Here this problem will be considered based on the general CL model (12).

C. Interface dynamics

Finishing the general part of this work let us consider the interface dynamics as described by the CL model. The law of the interface motion can be derived by considering the free energy variation at the motion of the interface. Considering the interface position variation $\vec{\rho}' = \vec{\rho} + \vec{\xi}$ and taking into account the relations (v_n is the normal to the interface velocity component of the domain boundary, k is the curvature of the interface taken constant across the film, S is the surface area of the sample, and l is the countour L arclength)

$$\delta\rho_n = \frac{1}{S} \sum_i \int_{L_i} v_{ni} dl\, dt,$$

$$\delta\sigma d \int_{L_i} dl = \sigma d \int_{L_i} k_i v_{ni} dl\, dt,$$

$$\delta \frac{1}{8\pi} \int \tilde{\vec{H}}^2 dV = 2M^2 \sum_i \int_{L_i} v_{ni} dl\, dt \int_{S_n} dS' J(\vec{\rho} - \vec{\rho}', d),$$

the free energy variation is expressed as follows:

$$\frac{dF}{dt} = d\sum_i \left(\frac{H_c^2}{8\pi} - \frac{H_0^2}{8\pi\rho_n^2}\right)\int_{L_i} v_{ni}dl + \sigma d\sum_i \int_{L_i} k_i v_{ni} dl + 2M^2 \sum_i \int_{L_i} v_{ni}dl \int_{S_n} dS' J(\vec{\rho}-\vec{\rho}',d). \quad (20)$$

Since $dF/dt = -TdS_t/dt$ (S_t is the total entropy) this gives the following kinetic law for the interface motion:

$$v_{ni} = -\frac{1}{\zeta}\left(\frac{H_c^2}{8\pi} - \frac{H_0^2}{8\pi\rho_n^2} + \sigma k_i + \frac{2M^2}{d}\int_{S_n} dS' J(\vec{\rho}-\vec{\rho}',d)\right). \quad (21)$$

Here ζ is the kinetic coefficient. At equilibrium when the interface does not move the right side of Eq. (21) is equal to zero. This condition is equivalent to the condition of the absence of pressure in a system of domains of the normal phase with equal size:

$$p = -\frac{\partial F}{\partial V_n} = -\frac{1}{V}\frac{\partial F}{\partial \rho_n}.$$

Thus one of the conditions determining the structure of the intermediate state is $\partial F/\partial\rho_n = 0$. This condition was not considered in the previous papers describing the intermediate state in the framework of the CL model.[19,26] The equivalent form for the law of interface motion allowing a physical interpretation in terms of the Lorentz force on the superconducting currents is given in Appendix A. Another condition for the determination of the pattern of the intermediate state comes from the minimization of the free energy with respect to the period of the structure. Necessary relations and the results of numerical calculations are given in Sec. III.

III. STRIPE AND HEXAGONAL PHASES

In this section we will determine the free energy, the period, and the domain sizes of the bubble hexagonal phase and the stripe phase.

A. Stripe phase

Let us first consider the case of the stripe phase, which is simpler. Resolving the magnetostatic problem of the magnetic field distribution created by the periodic system of the magnetized stripes with width $2w$ and period a for the magnetic energy we obtain

$$\frac{1}{8\pi}\int \tilde{\vec{H}}^2 dV = 2\pi\sigma S\left[\frac{1}{\rho_n^2}\left(\frac{H_0}{H_c}\right)^2 \mathrm{Bm}\frac{a}{d} \times \sum_{n=1}^{\infty} \frac{\sin^2(2\pi nw/a)[1-\exp(-2\pi nd/a)]}{\pi^3 n^3} + \frac{1}{\rho_n^2}\mathrm{Bm}\left(\frac{H_0}{H_c}\right)^2\left(\frac{2w}{a}\right)^2\right]. \quad (22)$$

The magnetic field strength H_n in the normal phase is fixed by flux conservation: $H_0 = \rho_n H_n$, where $\rho_n = 2w/a$. Using the relation in Ref. 38,

$$\sum_{k=1}^{\infty} \frac{[1-(-1)^k\cos(\pi kz)]}{k^3}[1-\exp(-kx)] = -\frac{x^2}{2}\int_0^1 (1-t)\ln\left(1+\frac{\cos^2(\pi z/2)}{\sinh^2(xt/2)}\right)dt + \frac{x\pi^2(1-z^2)}{4}, \quad (23)$$

it is convenient to rewrite the expression for the free energy of the stripe phase in the following form:

$$F_s = F_{supra} + 2\pi\sigma S\left\{\mathrm{Bm}\rho_n + \left(\frac{H_0}{H_c}\right)^2\frac{\mathrm{Bm}}{\rho_n} + \frac{d}{\pi a} + \left(\frac{H_0}{H_c}\right)^2\frac{1}{\rho_n^2}\mathrm{Bm}\left[\rho_n - \frac{d}{\pi a}\int_0^1 (1-t) \times \ln\left(1+\frac{\sin^2(\pi\rho_n)}{\sinh^2(\pi dt/a)}\right)dt\right]\right\}. \quad (24)$$

Before considering the results following from the general expression of the magnetic energy of the stripe phase (24) let us consider the limiting case $d\to\infty$ of the CCL model. Taking into account the relations

$$\pi^2\rho_n(1-\rho_n) = \int_0^{\infty} \ln\left(1+\frac{\sin^2(\pi\rho_n)}{\sinh^2(y)}\right)dy$$

and

$$\sum_{k=1}^{\infty}\frac{\sin^2(\pi k\rho_n)}{k^3} = \int_0^{\infty} y\ln\left(1+\frac{\sin^2(\pi\rho_n)}{\sinh^2(y)}\right)dy,$$

we obtain for the energy of the stripe phase

$$F_s = F_{supra} + 2\pi\sigma S\left[\mathrm{Bm}\rho_n + \left(\frac{H_0}{H_c}\right)^2\frac{\mathrm{Bm}}{\rho_n} + \frac{d}{\pi a} + \mathrm{Bm}\left(\frac{H_0}{H_c}\right)^2 + \frac{1}{\rho_n^2}\left(\frac{H_0}{H_c}\right)^2\mathrm{Bm}\frac{a}{\pi^3 d}\int_0^{\infty} y\ln\left(1+\frac{\sin^2(\pi\rho_n)}{\sinh^2(y)}\right)dy\right]. \quad (25)$$

In this case minimization with respect to the period can be carried out directly, which gives the relation

$$\left(\frac{d}{a}\right)^2 = \frac{1}{\rho_n^2}\left(\frac{H_0}{H_c}\right)^2\mathrm{Bm}\frac{1}{\pi^2}\int_0^{\infty} y\ln\left(1+\frac{\sin^2(\pi\rho_n)}{\sinh^2(y)}\right)dy.$$

This relation gives the result, which is close to that obtained in Landau's classical paper,[20] as shown in Refs. 19 and 26.

Minimization of the free energy with respect to the two variables ρ_n and a is carried out by the downhill simplex method. The dependence of the width of the stripes on the magnetic field strength is shown in Fig. 1 (Bm=5 and 300). In the limit of vanishing field strength the thickness of the stripes has a limiting value which can be determined as follows. Differentiating the free energy expression with respect to the period the following equation is obtained:

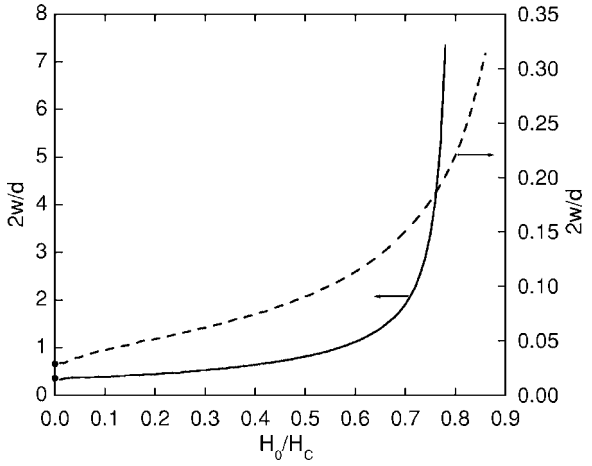

FIG. 1. Relative width of the stripe of the normal phase in dependence on the magnetic field strength: Bm=5 (solid curve, left scale) and 300 (dashed curve, right scale).

$$\left(\frac{H_0}{H_c}\right)^2 \frac{1}{\rho_n^2}\mathrm{Bm}\int_0^1 t\,\ln\left(1+\frac{\sin^2(\pi\rho_n)}{\sinh^2(\pi dt/a)}\right)dt = 1. \quad (26)$$

In the limit $H_0 \to 0$, when $H_0=\rho_n H_c$ and $a\to\infty$ relation (26) gives the following equation for the limiting value of the relative width of the stripes of normal phase $\delta=2w/d$:

$$\mathrm{Bm}\frac{1}{2}\left[\delta^2 \ln\left(1+\frac{1}{\delta^2}\right)+\ln(1+\delta^2)\right]=1. \quad (27)$$

This is exactly the equation for the relative width of stripes arising at magnetic-field-induced phase separation of magnetic colloids found from thermodynamic arguments in Ref. 39. At this particular value of the stripe width its effective surface tension as shown in Ref. 37 is exactly equal to zero. This is correlated with the fact that arising stripes of the normal phase are usually buckled. The value of the relative stripe width as shown by the black dots in Fig. 1 coincides well with the width of the stripes in the limit of low field found from the numerical minimization of the free energy given by the relation (24). The comparison of the calculated dependence of the stripe width with experiment is carried out in Sec. V. The volume fraction of the stripe phase in dependence on the external magnetic field strength is shown in Fig. 2 (Bm=5 and 300). For the small value of the magnetic Bond number Bm=5 the dependence of the volume fraction deviates from the simple linear law $\rho_n=H_0/H_c$ corresponding to the case when the interactions between the domains of the normal phase can be neglected. As shown in Sec. IV D it corresponds to the experimental results quite well.

B. Hexagonal phase

According to relations (10)–(12) the energy of the hexagonal lattice of the cylindrical domains of the normal phase is expressed as follows:

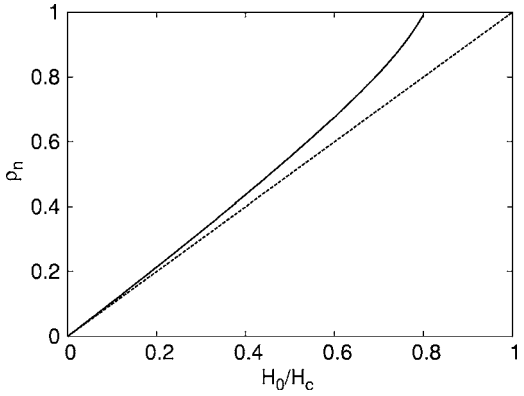

FIG. 2. Volume fraction of the stripes of the normal phase in dependence on the magnetic field strength: Bm=5 (solid curve) and 300 (dashed curve).

$$F_h = F_{supra} + V\frac{1}{8\pi}H_c^2\rho_n + V\frac{1}{8\pi}H_n^2\rho_n + N2\pi\sigma dR + NM^2\int dS\int dS' J(\vec{\rho}-\vec{\rho}',d) + NM^2\sum_{n_1,n_2\neq 0}\int dS\int dS' J(\vec{\rho}-\vec{\rho}'-\vec{\rho}_n,d). \quad (28)$$

Here N is the number of domains, and $\vec{\rho}_n=a(n_1\vec{e}_1+n_2\vec{e}_2)$, where $\vec{e}_1$ and $\vec{e}_2$ are basic vectors of the elementary cell of the hexagonal lattice with period a. The number of domains N is expressed using the period of the structure as $N=2S/\sqrt{3}a^2$, where S is the area of the film. As a result the free energy of the hexagonal pattern can be written as follows

$$F_h = F_{supra} + 2\pi\sigma S\left[\left(\frac{H_0}{H_c}\right)^2\frac{\mathrm{Bm}}{\rho_n^2}N_{dm}(x,y)+\frac{xy}{\sqrt{3}}+\mathrm{Bm}\,\rho_n + \left(\frac{H_0}{H_c}\right)^2\frac{\mathrm{Bm}}{\rho_n}\right]; \quad (29)$$

here $\rho_n=2\pi R^2/\sqrt{3}a^2$. The effective demagnetizing field coefficient $N_{dm}(x,y)$ as function of parameters $x=d/a$ and $y=2R/a$ is given in Appendix B. For its calculation the relation

$$\frac{1}{p}=\frac{2}{\sqrt{\pi}}\int_0^{1/2\sqrt{\tau}}\exp(-t^2p^2)dt+\frac{1}{p}\mathrm{erfc}\left(\frac{p}{2\sqrt{\tau}}\right)$$

is used and the sums are calculated according to the Evald summation technique. Minimization of the free energy with respect to the variables ρ_n and a is carried out by the downhill simplex method. The radius of the domain of the normal phase in dependence on the magnetic field is shown in Fig. 3 (Bm=5 and 300). Looking at these curves we pay attention to the limiting value of the radius when the applied magnetic field H_0 goes to zero. In this limit the density of the normal phase is small and interactions between domains can be neglected. In this case the free energy has the following functional dependence:

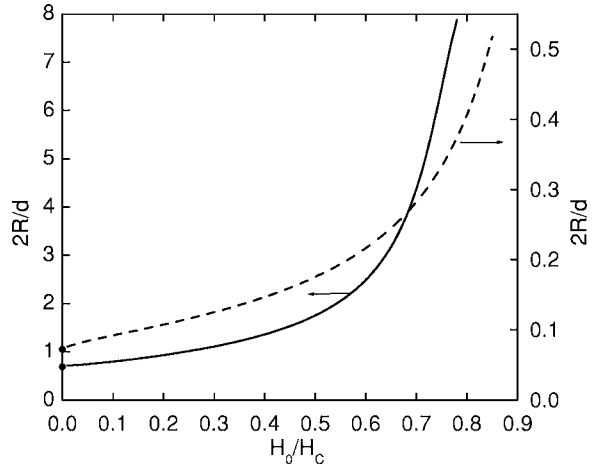

FIG. 3. Relative diameter of the cylindrical domain of the normal phase in dependence on the magnetic field strength: Bm=5 (solid curve, left scale) and 300 (dashed curve, right scale).

$$F_h = F_{supra} + 2\pi\sigma SG\left(\left(\frac{2\sqrt{3}\rho_n}{\pi}\right)^{1/2}\frac{a}{d}, \rho_n, \mathrm{Bm}, \frac{H_0}{H_c}\right).$$

From the last expression it follows that in the limit of the vanishing density of the normal phase the minimization with respect to the period is equivalent to the minimization of the free energy with respect to the radius of the domain of the normal phase. This gives the equation[29] ($k^2=(2R)^2/[d^2+(2R)^2]$):

$$\mathrm{Bm} = \frac{3(1-k^2)}{2k^2[1+(k^2-2)E(k)/k^3+2(1-k^2)K(k)/k^3]}. \quad (30)$$

The relation (30) in the limit $k\to 0$ fairly well describes the existing experimental data.[29]

An important issue for understanding the morphology of the intermediate state concerns the comparison of the energies of the hexagonal and stripe phases. The energy difference between the stripe and the hexagonal phases for the two values of the magnetic Bond number is given in Fig. 4 (Bm=5 and 300). Although the energies are very near each other (the difference does not exceed 1%) there exists a transition from the hexagonal to the stripe phase. Already with the illustrations shown in Fig. 4, a few comments can be made: (i) the transition field only slightly varies with the magnetic Bond number; (ii) for large magnetic Bond numbers the free energies of the stripe and hexagonal phase are much closer than for small Bond numbers.

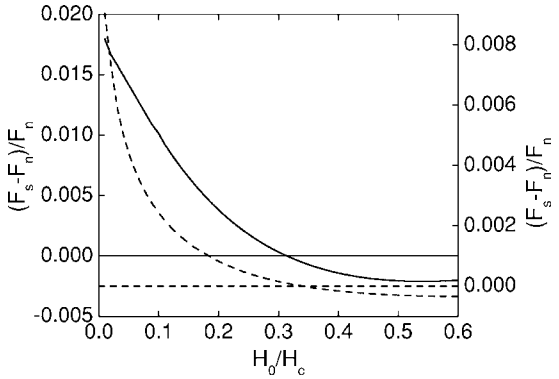

FIG. 4. The energy difference between the stripe and the hexagonal phases: Bm=5 (solid curve, left scale) and 300 (dashed curve, right scale).

In the next sections we report experimental results concerning the growth of bubbles and lamellae and discuss them in view of the theoretical predictions of Secs. II and III.

IV. IMAGING THE INTERMEDIATE-STATE STRUCTURES

A. Experimental setup and samples

The IS flux pattern in SC films was studied with the high-resolution Faraday microscopy imaging technique. A magneto-optic layer (MOL) is placed against the SC film, which allows one to map the normal component of the magnetic induction at the surface of the slab. The SC samples consisted of lead and indium films. Lead samples were cut out from 25 and 120±1 μm thick foils of Goodfellow 99.9% purity annealed lead. The thinnest indium samples were grown by Joule evaporation directly onto the MOL. The thicknesses of evaporated indium samples were 0.6, 1.1, 1.5, 2.2, and 10.0±0.1 μm. Other indium samples were cut out from 33± 3 μm and 112± 3 μm thick foils of Goodfellow 99.8% purity indium. Investigating samples of various thicknesses d from materials with different interface energy parameters Δ aimed at exploring the full range of magnetic Bond numbers $\mathrm{Bm}=d/2\pi\Delta(T)$ over which the nonbranching IS pattern is expected to be observed.[23,40] As $\Delta(0)=0.056$ and 0.33 μm, for Pb (Ref. 13) and In[41], respectively, the corresponding range of magnetic Bond numbers extends from 0.3 to 350.

The MOL used to study the lead slabs was made of EuS. It was fabricated by Joule-effect evaporation on a 0.4 mm glass substrate and had a thickness of 1500 Å. A 600 Å thick Al mirror was evaporated on top of it. The lead slabs were compressed against the mirror. Generally EuS presents self-magnetic ordering. However, we did not observe magnetic domains, presumably due to a rather high content of oxygen. For the indium slabs, the MOL consisted of a CdMnTe/CdMgTe quantum well structure grown by molecular beam epitaxy.[42] CdMnTe is well known to exhibit a large Faraday rotation due to the giant Zeeman splitting of the excitonic transition. The advantageous point of these MOLs is that there is no self-magnetic ordering due to the paramagnetic behavior of the Mn ions. Furthermore it is easy to increase Faraday rotation by designing the MOL as an optical cavity (metal/semiconductor/vacuum) and by placing the quantum wells at antinodes of the electric field.[43] Here indium serves as both the SC layer and the cavity back mirror. The peak Faraday angle was found to vary linearly with the applied magnetic field with a slope of 54.4 deg T^{-1} at the quantum well lowest excitonic transition.

The samples were placed in an immersion-type cryostat in pumped liquid helium. The microscope objective with numerical aperture 0.4 is placed in the vacuum part of the cryostat and can be controlled from outside. The optical setup is

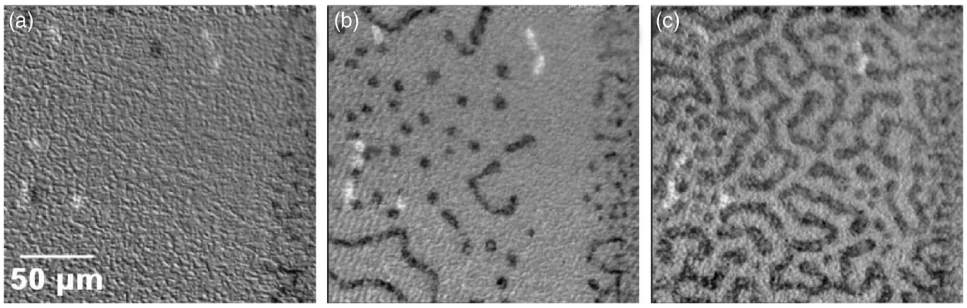

FIG. 5. IS pattern in a 10 μm indium sample for values of the reduced magnetic field H_0/H_c =0.056 (a), 0.132 (b), and 0.378 (c) at $T=2K$ (Bm=3.1). The edge of the sample is along the right edge of the images.

similar to a reflection polarizing microscope. The indium samples were illuminated with linearly polarized light from a Ti-sapphire laser, through a rotating diffuser in order to remove laser speckle. In the case of lead samples a tungsten lamp with an interference filter centered at 700 nm was used as a light source. Reflected light from the sample passes through an analyzer uncrossed by $\approx 15°$ and is focused onto a charge-coupled device camera. The spatial resolution of 1 μm is limited by the numerical aperture of the microscope. The magnetic resolution is 8 mT.[42] The samples were first zero-field cooled; then they were subjected to a perpendicular magnetic field H_0 whose maximum value is 60 mT. After cycling the field, some trapped flux is observed at zero field.

B. Normal-state bubbles and lamellae

Figure 5 shows typical IS structures observed in the 10 μm indium sample at three values of the reduced applied magnetic field H_0/H_c. Raw images were corrected in order to remove reflectivity fluctuations of the MOL using a reference image taken at $H_0=0$.[42] The flux-bearing NS domains and SC areas appear in black and in gray, respectively. The few white spots correspond to NS domains that remain trapped in the sample at $H_0=0$. At very low H_0 only the movement of trapped flux consisting of very few bubbles is observed [Fig. 5(a)]. Increasing H_0 results in an increase of the density of the NS phase due to the penetration of magnetic flux from the edges of the slab. At low applied field [Fig. 5(b)], the NS domains mainly consist of circular bubbles. For all the samples studied NS bubble domains were systematically observed to form the early stage of the IS. At higher applied field, lamella-shaped domains appear and form labyrinthine structures [Fig. 5(c)]. The coexistence of bubbles and lamellae as observed in Fig. 5(b) makes difficult a separate determination of their respective quasiperiods. In order to investigate the field dependence of these patterns, as developed below, it is more convenient to measure the diameter of bubbles and the width of lamellae.

C. Flux inhomogeneities and pinning

Whereas the IS model developed above assumes regular domain structures, the observed flux distributions are disordered and a global flux inhomogeneity is observed on the scale of the image at low field value [Fig. 5(b)]. The contribution of the pinning of the domains to the disorder can be evidenced by substracting the IS images obtained for two successive values of the field. Thus one can follow the movement of flux-bearing structures. Flux tubes very often move by a distance equal to their diameter. This suggests that domain walls are pinned by point centers. By locating those centers for successive values of the applied field, we obtain a map of the pinning centers. The measured concentration is about $9\times 10^{-4}\mu m^{-2}$. A comparison of this map with the flux structure in the lamella regime, at higher field (Fig. 6), shows that about 60% of the pinning centers are found on one interface of a lamella. Thus pinning is found to contribute to the positioning of bubbles and to the labyrinthine structure of the lamellae in addition to shape instabilities.[26,28] Hysteresis or at least a modification of the field dependence of the domain period and size is also likely to occur.

At low field values, as observed in Fig. 5(b), the magnetic flux is globally not homogeneous. A full diamagnetic band, about 50 μm wide, separates the IS structure present on the slab edge from the IS structure present in the interior. This diamagnetic band results from the existence of an energy barrier of geometrical origin.[25,31,32] The NS domains originate from the IS structure on the edges of the sample. They have to cross the diamagnetic band to penetrate into the sample. This is no longer the case at higher field value [Fig. 5(c)]. The diamagnetic band has disappeared and NS lamellae are connected to the edge of the sample. This suggest that

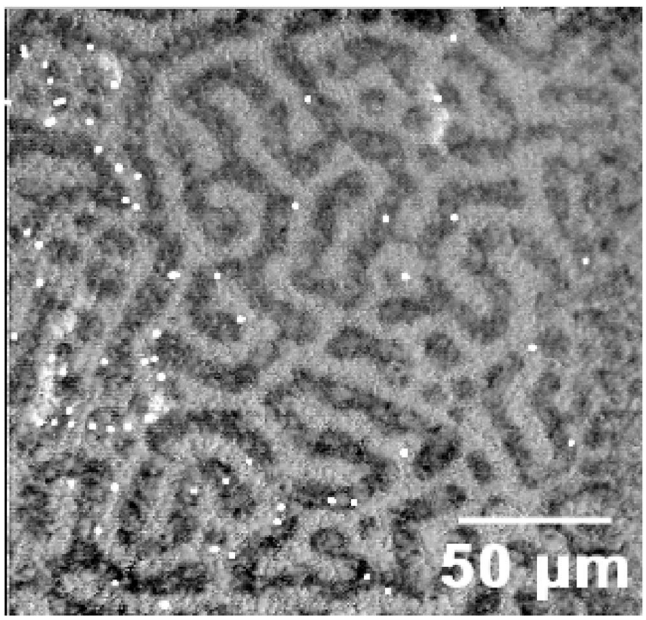

FIG. 6. Pinning sites (white spots) overlaying the IS pattern at $H_0/H_c=0.416$.

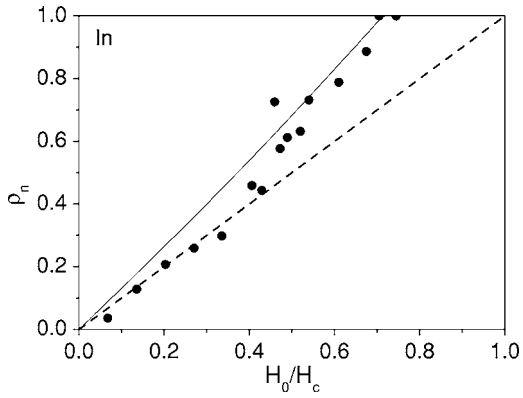

FIG. 7. Area fraction of NS domains ρ_n for the 2.2 μm indium sample at 1.8 K as a function of the reduced applied magnetic field. The black circles are the experimental values obtained from the analysis of images of the magnetic flux. The full line is the calculated area fraction for a stripe lattice in the CL model with Bm $=0.73$. The dashed line corresponds to $\rho_n=H_0/H_c$.

the formation and penetration mechanisms of NS domains are different at low field values where bubbles are mainly observed and at high field values where lamellae form the dominant pattern.

D. Area fraction of NS domains

Previous IS models usually assume that the magnetic field h_n in the NS domains is equal to the thermodynamical critical field H_c.[20,26] This is an approximate result obtained by neglecting interface energy and stray field energy terms, which are much smaller than bulk energy terms [see Eq. (12)], in the minimization of the free energy. When all terms are properly taken into account, h_n is found to be smaller than H_c as discussed in Sec. III. In order to determine the importance of this effect we measured the area fraction ρ_n of NS domains as a function of the applied field. Figure 7 presents the result obtained for the 2.2 μm indium sample (Bm$=0.73$). Owing to the large demagnetizing factor in our film samples, ρ_n increases as soon as H_0 reaches a few percent of H_c. At low field, ρ_n is equal to H_0/H_c, i.e. $h_n=H_c$ in NS domains. Then ρ_n progressively deviates from the linear behavior: h_n becomes smaller than H_c. The transition to the NS ($\rho_n=1$) occurs at an effective critical field lower than $H_c(\approx 0.7H_c)$. Figure 7 also shows the variation of ρ_n calculated in the CL model for stripes (the curve for bubbles, not shown here, is very similar). The experimental findings are qualitatively reproduced by the theoretical results. In agreement with the predictions we found that the effective critical field increases toward H_c for increasing sample thickness. For the 112 μm indium sample (Bm$=37$) the effective critical field was found equal to $\approx 0.9H_c$. This indicates that, for finding the equilibrium condition of the system, the interface energy and the stray field energy cannot be neglected at large applied field and for a magnetic Bond number up to a few tens. A detailed study of this effect, which is beyond the scope of this paper, will be presented in a forthcoming publication.[44]

V. THE GROWTH OF LAMELLAE

A. Field-dependent width of lamellae

In order to determine how accurately the CL and CCL models describe the magnetic interaction between domains, let us first analyze the growth of lamellae. Figure 8 shows the mean width of lamellae as a function of the reduced applied magnetic field $H_0/H_c(T)$ for the 10 μm indium sample (left figure) and the 120 μm lead sample (right figure). Error bars represent the full width at half maximum of the size distribution. The dashed (solid) line is the prediction of the CL (CCL) model for a one-dimensional lattice of infinitely long stripes. $H_c(T)$ is assumed to follow a Bardeen-Cooper-Schrieffer temperature variation: $H_c(T)=H_c(0)[1-(T/T_c)^2]$. $H_c(0)$ equals 28.2 and 80.3 mT for indium and lead, respectively. T_c is 3.4 K for indium and 7.2 K for lead. The variation of $\Delta(T)$ with temperature is assumed to follow

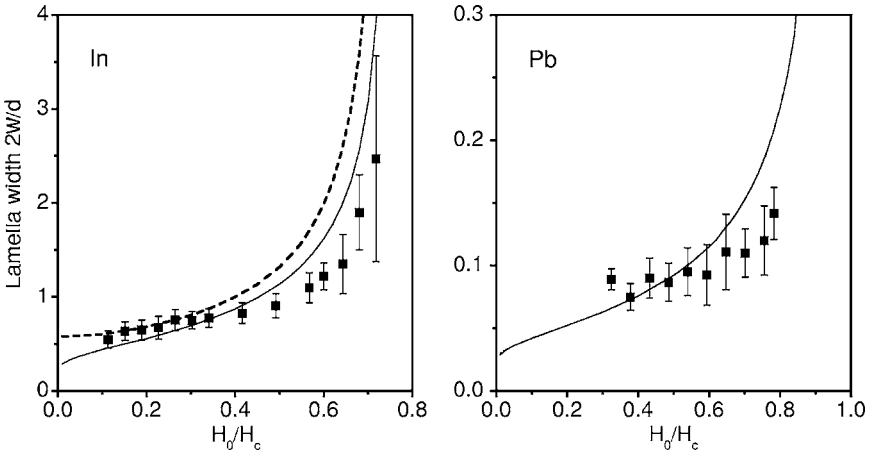

FIG. 8. Mean lamella reduced width $2w/d$ as a function of the reduced magnetic field $H_0/H_c(T)$ for a 10 μm thick In slab (left) and a 120 μm thick Pb slab (right) at $T=2$ K. The error bars represent the full width at half maximum of the distributions of lamella width. The dashed (solid) curve represents the calculated equilibrium width using the CL (CCL) model with $\Delta(T)=0.51$(Bm$=3.1$) and 0.066 (Bm $=290$) for In and Pb, respectively. The two curves coincide for Bm$=290$.

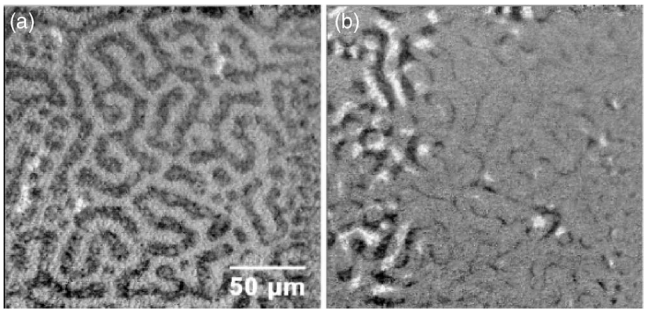

FIG. 9. (a) Image of the IS pattern in the 10 μm indium sample at $H_0/H_c=0.41$ and $T=2$ K(Bm=3.1). (b) Image (a) is subtracted from the one taken at $H_0/H_c=0.45$ in order to reveal flux movement.

the empirical law $\Delta(T)=\Delta(0)/\sqrt{1-(T/T_c)}$ proposed in Ref. 41. We use $\Delta(0)=0.056$ μm for Pb,[13] and $\Delta(0)=0.33$ μm for In.[41] For the lowest H_0/H_c values ($H_0/H_c<0.4$ for indium and $H_0/H_c<0.65$ for lead), the predicted and the measured widths present a reasonable agreement. It is important to notice that the magnetic Bond number is varied by two orders of magnitude (Bm=3.1 for indium and 290 for lead) and that there is no adjustable parameter. The predictions of the CL and the CCL models are identical for Bm=290. For Bm=3.1, the predicted width is smaller for the CCL than for the CL model. Given the experimental error bars, both models provide a reasonable description. The mean width of the lamellae increases with H_0/H_c almost as predicted. This indicates that the observed lamellae patterns can be described by a succession of equilibrium states, the growth of the lamellae being essentially the result of the competition between long-range and short-range interactions. This most likely results from the fact that a large number of lamellae are connected to the edges of the slab, thus allowing the magnetic flux to penetrate continuously from the exterior.

For the highest H_0/H_c values, the width of the lamellae continues to grow. However, the measured values are smaller than the predictions. Indeed, in this regime, for indium the IS pattern consists of a disordered network of SC lamellae separated by large NS domains whose width is not well defined (the distribution of width values is represented by the error bars) and for lead there is also a non-negligible fraction of bubbles in the NS phase. Therefore we cannot expect very good agreement with theoretical predictions made for a perfect stripe lattice.

B. Growth and jumps

The evolution of the lamellae pattern can be put in evidence by comparing successive images taken for increasing field values. Figure 9(a) shows the maze pattern of lamellae at a reduced applied field $H_0/H_c=0.41$ for the 10 μm indium sample. Figure 9(b) shows the result of the subtraction of this image from the one recorded at $H_0/H_c=0.45$. White areas show places from which magnetic flux has moved away and black areas places where it has arrived. The increase of the width of lamellae which are connected to the edge is revealed by very thin black filaments on the center and right parts of Fig 9(b). The jumps of lamellae appear as adjacent black and white structures on the left part of Fig. 9(b).

At large field most lamellae are connected to the edges. Therefore it is easy to understand that their growth can be continuous due to the reversible penetration of magnetic flux from the exterior. At low field, lamellae have to cross the diamagnetic band to penetrate far into the interior of the sample. They are often no longer connected to the edge. However, their mean width also increases with the field. Since lamellae have several degrees of freedom (width, length, and buckling), the length and buckling very likely become adjusted in such a way that the width is nearly equal to the equilibrium one. This is reasonable since the energy of an isolated lamella is governed mainly by its width and almost does not depend on its length or buckling.[26]

VI. THE IMPEDED GROWTH OF BUBBLES

A. Field-independent diameter

The growth of bubbles presents different characteristics as compared to the growth of lamellae. Figure 10 shows the mean diameter of bubbles for the 10 μm indium slab (left) and the 120 μm lead slab (right) as a function of the applied magnetic field. The dashed (solid) curve represents the equilibrium diameter calculated using the CL (CCL) model. Again the CL and CCL models give identical curves for the lead sample with a large magnetic Bond number. Contrary to

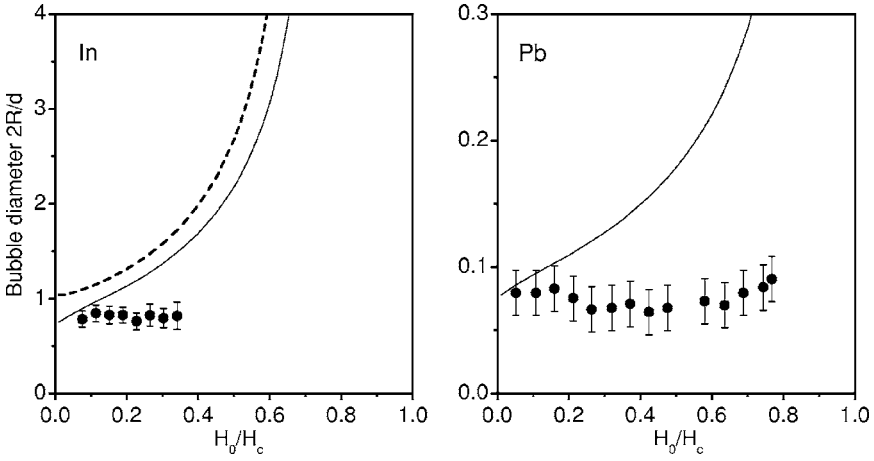

FIG. 10. Mean bubble reduced diameter $2R/d$ as a function of the reduced magnetic field $H_0/H_c(T)$ for the 10 μm thick In slab (left) and the 120 μm thick Pb slab (right) at $T=2$ K. The dashed (solid) line represents the equilibrium diameter calculated using the CL (CCL) model with Bm=3.1 for indium and 290 for lead. The two curves coincide for Bm=290.

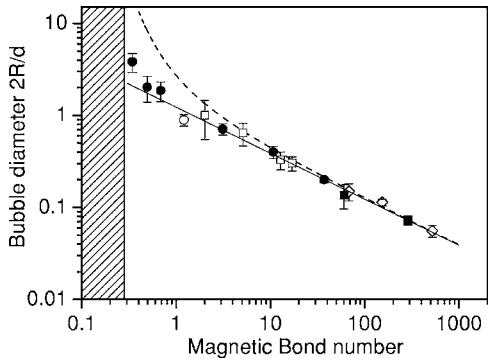

FIG. 11. Log-log plot of the reduced bubble diameter $2R/d$ as a function of the magnetic Bond number $d/(2\pi\Delta)$. The filled circles and squares were obtained with In and Pb slabs, respectively. The empty lozenges, squares, and circles are reported from Ref. 22, 24, and 25 for Hg, Pb, and In, respectively. The shaded region corresponds to type-II superconductivity for very thin slabs. The theoretical curves represent the equilibrium bubble diameter in the limit $H_0 \to 0$, i.e., neglecting interbubble interactions: the dashed curve is obtained using the CL model, the solid curve using the CCL model (see text).

the lamella width, the bubble diameter stays almost constant as the field increases, i.e., as the volume fraction of the normal phase increases. This indicates that the mean diameter is independent of the magnetic interactions between NS domains. Indeed the measured diameter tends to the equilibrium value predicted by the CCL model for $H_0 \to 0$, that is, in a situation where interbubble interaction can be neglected. This suggests that the CCL model might correctly describe the bubble mean diameter, provided that it is used in the zero-field limit.

B. The master curve

Since the lack of dependence of the bubble mean diameter on the interdomain magnetic interaction is demonstrated for two samples that differ much in their thicknesses and interface parameters, one may suspect that this behavior has a general character. In order to clarify this point we investigated lead and indium samples of various thicknesses and we collected earlier data on Pb, Hg, and In from the literature.[22,24,25,45] In Fig. 11 we plot the mean bubble diameter in units of the sample thickness d as a function of the magnetic Bond number $\mathrm{Bm}=d/(2\pi\Delta)$. All the data gather on a single master curve. This proves that (i) the mean diameter does not depend on the specificities (shape of the edges, pinning properties) of the samples studied and (ii) the thickness d and the interface width Δ are the only parameters that control the bubble system. The shaded area below a critical Bond number $\mathrm{Bm}_c=d_c/(2\pi\Delta)$ represents the region where samples become type-II superconductors. Our thinnest indium sample ($d=0.6$ μm) falls in this range. Indeed we did not observe NS domains in this sample although their calculated size is larger than the spatial resolution. The interface energy should drop to zero and become negative in a very narrow range of thickness around d_c.

Let us compare the master curve with the theoretical predictions for the equilibrium radius in the limit $H_0 \to 0$, i.e., neglecting interbubble magnetic interaction. The dashed curve of Fig. 11 represents the diameter calculated in the framework of the CL model using Eq. (30). A good quantitative agreement is found for $\mathrm{Bm} > 10$. On the contrary, for $\mathrm{Bm} < 10$ the predicted diameter is larger than the measured one. The discrepancy increases when Bm decreases (for $\mathrm{Bm}=0.5$ the predicted and measured diameters differ by a factor of ≈ 4). The CL model is unable to describe accurately the bubble pattern for small Bond numbers. The solid curve of Fig. 11 represents the equilibrium diameter calculated using the CCL model [Eq. (16)]. This prediction is in good agreement with the measurements over three orders of magnitude of the magnetic Bond number ($\mathrm{Bm}=0.5$–500). This demonstrates that the CCL model accurately describes the bubble pattern. We can conclude that the bubble mean diameter is solely determined by the competition between the interface energy and the energy of the stray field created by the screening current flowing around the bubble. Moreover, the CCL model, which takes into account the shielding of field lines by surface currents, describes experimental results much better than the CL model, for which current loops are interacting as in the free space.

The impeded growth of bubbles most likely results from the nature of the SC phase. Let us consider the time variation of the magnetic flux Φ in a bubble isolated in the SC matrix. The Maxwell-Faraday equation gives us $d\Phi/dt = -\oint \vec{E} \cdot \vec{dl}$ with $\vec{E}$ the electric field. The contour of the line integral is taken as a closed loop encircling the bubble in the SC matrix at a distance larger than the penetration depth. As the electric field $\vec{E}$ is zero in the SC phase the magnetic flux Φ within the NS bubble must remain constant.[33] Since the field h_n in the NS areas is equal to the critical field in the limit of small density of the normal phase (Sec. III) the area of the isolated NS bubble must remain constant. Consequently, flux variation in an isolated bubble and therefore size variation can only result from the movement of an incoming NS domain.

For the bubble size to grow, not only has another NS domain to reach the bubble, it has to merge with it. However, the fusion of two NS domains is impeded by their repulsive interaction.[46] Moreover, the formation of bubbles of size much smaller than the equilibrium one is very unlikely due to the positive interface energy. As a consequence the continuous growth of isolated NS domains with the applied field is hindered.

The fact that isolated bubbles cannot grow in size as the field increases is not sufficient to explain that the mean diameter of the bubble distribution also does not increase with the applied field. We would expect that, the higher the field value at which the bubbles penetrate into the sample, the larger their diameter. Then the average diameter should increase with the field, though at a smaller rate than predicted. Actually, as will be discussed below, it is often observed that a large fraction of the observed bubbles penetrates into the sample in a single burst at low field and that further flux penetration is dominated by lamellae. Furthermore, bubble shape instabilities, which are theoretically and experimentally actively studied in various systems,[3,5,18,26] very likely

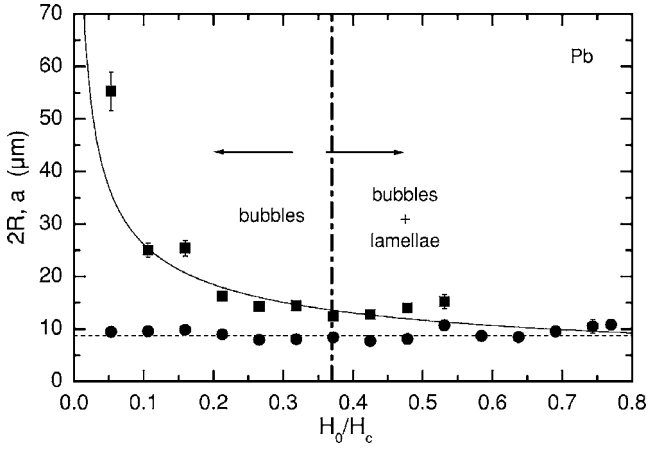

FIG. 12. Mean diameter $2R$ (filled circles) and mean distance a (filled squares) between bubbles in the 120 μm Pb sample at 2 K (Bm=290). The solid line represents the mean distance calculated with a constant diameter (dotted line), assuming global flux conservation $\rho_n = H_0/H_c$.

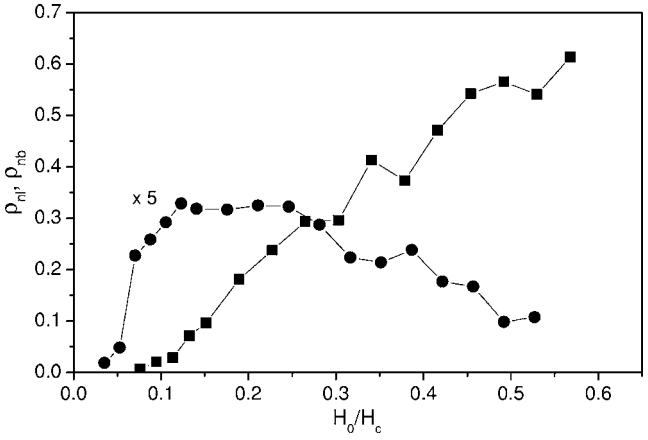

FIG. 13. Area fraction of NS bubbles (black circles) and NS lamellae (black squares) as functions of the reduced applied field for the 10 μm thick indium sample at 2 K.

play a major role in the fast transformation of large-diameter bubbles into lamellae therefore making large-size bubbles unobservable.[44]

C. Close-to-equilibrium system

Let us examine how far from equilibrium the bubble system is. Figure 12 shows the mean diameter and mean distance between bubbles as a function of the field for the 120 μm lead sample. The full line represents the period of a hexagonal lattice built from bubbles with their constant diameter assuming flux conservation, i.e., the volume fraction of NS domains ρ_n is equal to H_0/H_c. One can see that the mean distance between bubbles varies with the field in good agreement with the calculated period. This means that interaction between bubbles, which is unimportant for fixing their size, serves to adjust their distance in such a way that the constraint of global flux conservation is satisfied. The energy calculated for such a lattice [Eq. (12)] is at most only 0.5% larger than the energy of the equilibrium lattice. The reason is that bulk energy terms that depend on ρ_n but not on the period are much larger than the interface and stray-field energy terms that depend on both ρ_n and the period. Therefore, although bubbles keep their zero-field diameter, the bubble system is only slightly out of equilibrium.

VII. TRANSITION FROM BUBBLE TO STRIPE PATTERN

After having investigated the size variations of lamellae and bubbles, it is interesting to study their respective concentrations and to determine whether there is some experimental evidence of a bubble-to-lamella transition as predicted in Sec. III of this paper. Bubble patterns are systematically observed to form in the early stage of the IS whereas the lamellae pattern dominates when H_0/H_c increases (see Fig. 5). Typical variations of the area fraction of bubbles ρ_{nb} and lamellae $\rho_{nl}(\rho_n = \rho_{nb} + \rho_{nl})$ are shown in Fig. 13 for the 10 μm indium sample. The formation of domains starts for $H_0/H_c > 0$, due to the finite width of the slab. Lamellae appear at $H_0/H_c = 0.075$ while bubbles are already present in the sample. The fraction of lamellae ρ_{nl} then increases monotonically with the field. In contrast, the fraction of bubbles ρ_{nb} only increases over a reduced range of H_0/H_c values and reaches a plateau. Within the plateau bubbles neither are created nor disappear. At the end of the plateau $(H_0/H_c = 0.26 \pm 0.04), \rho_{nb}$ starts to decrease. Bubbles are surrounded by other NS domains and cannot escape; they disappear by fusion with those domains. The fact that ρ_{nb} tends to zero when H_0 increases is experimental evidence of the bubble-to-lamella transition. The decreasing rate of ρ_{nb} was observed to vary systematically with the slab thickness d (i.e., the magnetic Bond number Bm). For the 2.2 μm (Bm=0.73) and the 10 μm thick In slabs $(\mathrm{Bm}=3.1), \rho_{nb} \to 0$ for $H_0/H_c \approx 0.45$ and ≈ 0.65, respectively. For the 112 μm thick In slab $(\mathrm{Bm}=37), \rho_{nb}$ decreases but bubbles are observed to remain present up to the end of the transition to the NS. These variations may be associated with the decrease of energy difference between the bubbles and the lamellae as Bm increases, as shown in Fig. 4. In order to get more insight into the bubble-to-lamella transition, it is important to determine the respective contributions of equilibrium state processes and of irreversible processes (such as the pinning of interfaces, the energy barrier against the fusion of domains,[46] and the geometrical barrier) on the variation of the bubble and lamellae concentrations. Since the bubble-to-stripe transition is predicted to be of first order, one expects a coexistence of the two types of patterns and continuous variations of ρ_{nb} and ρ_{nl}. Experimentally the coexistence of bubbles and lamellar patterns is effectively observed. After the plateau, the bubbles start to disappear for a well-defined value $H_0/H_c = 0.26 \pm 0.04$, close to the predicted value $H_0/H_c = 0.32$, for which the free energies of the bubble and lamellar lattices become equal. However, within the plateau bubbles are trapped and their growth is impeded. Moreover the penetration of bubbles occurs only when the diamagnetic band is present. Therefore ρ_{nb} and ρ_{nl} may differ from the equilibrium values and should depend on the mechanism of flux penetration on the edges of the sample.

These mechanisms may drive the early stage of the formation of bubbles and lamellae at low field and are not well understood.[36]

VIII. SUMMARY AND CONCLUSION

We have presented an extensive theoretical as well as experimental study of the formation of NS domains in the IS of type-I superconductors. The expression of the free energy of the intermediate state of the type-I superconductor derived in the current-loop approximation allows one to describe qualitatively and quantitatively the peculiarities of the morphology of the intermediate state observed in the experiments. Among the features studied in this paper we should mention the dependence of the domain size on the magnetic field, the nonlinear dependence of the volume fraction of the normal phase on the external field, and the existence of a transition between the hexagonal and the stripe phases. Different SC materials and slab thicknesses were used in order to cover more than three orders of magnitude of the magnetic Bond number (Bm=0.3–500), i.e., the full range over which nonbranching IS patterns are expected to occur. Experimentally we first analyzed the variation of the area fraction of the normal phase with the magnetic field and its spatial distribution within the SC slabs. At low field values, the magnetic field within the NS domains is shown to be equal to the thermodynamic critical magnetic field. Its value is reduced when the applied magnetic field increases because of the interface energy and the mutual interaction between domains. The contributions of the pinning of domain walls and of the geometrical barrier, which exists at low applied magnetic field values, have been shown to play a role in the inhomogeneity of the magnetic flux distribution at the early stage of flux penetration.

In order to determine to what extent the observed patterns correspond to equilibrium states, we have then analyzed the size variation of lamellae and bubbles. For lamellae, the field variation of their average width is found in reasonable agreement with the theoretical predictions. We show in addition that the evolution of the lamellar pattern results from both an increase of lamellae width and domain jumps, in order to satisfy the condition of flux conservation. The continuous growth of lamellae is ensured by the reversible flux penetration from the edges of the slab.

The case of bubbles is different. Their average diameter is found to be almost independent of the applied magnetic field, i.e., independent of the long-range magnetic interactions between domains. Under appropriate scaling the measured diameters are shown to gather onto a single master curve and to correspond to the equilibrium diameter of an isolated bubble. This diameter results solely from the competition between the Biot-Savart interaction of the screening current encircling the bubble and the SC-normal interface energy. A significantly better agreement is found with the CCL model than with the CL model, in particular for the thinnest SC slabs. This demonstrates that the NS domains cannot be simply modeled as current loops interacting as in the free space. The shielding of the magnetic field lines by surface screening currents has to be taken into account to accurately describe the stray-field magnetic energy.

Furthermore, the impeded growth of NS domains isolated in the SC matrix is shown to result from the nature of the SC phase. As long as the NS domains are completely surrounded by the SC phase, they cannot undergo flux variations. The growth of an isolated NS domain has to result from the merging with another NS domain. The combined effect of the repulsive magnetic interaction between domains and of the positive interface tension precludes the continuous growth of bubbles. The peculiar properties of the SC phase set a limit to the analogy between type-I superconductors and other two-phase, quasi-two-dimensional systems. In ferro- or ferrimagnetic thin films, like bubble garnets for instance, there is no similar constraint for flux variation. The up-magnetized isolated bubble domains can grow at the expense of the down-magnetized surrounding phase.

Finally, we found some experimental evidence for a bubble-to-lamella transition, as predicted theoretically. However, at low applied field, the concentrations of lamellae and of bubbles are shown to differ from equilibrium values. This sets a limit for the comparison between the experimental data and the predictions of the mean-field current-loop model. Indeed the respective concentrations of the bubbles and of the lamellae are likely to depend on the mechanism of flux penetration on the edges of the sample when the diamagnetic band is present.

Future studies will in particular aim at understanding the role of bubble shape instabilities in the observed distributions of bubbles and lamellae sizes at the early stage of flux penetration. On the opposite side, in the large field limit, work is in progress to study the transition from the IS to the NS as a function of the magnetic Bond number and compare the predictions of the CL and CCL models with experimental results.

APPENDIX A

The vector potential of the magnetic field created by superconducting currents circulating around the domain of the normal phase is expressed as follows:

$$\vec{A}' = \frac{1}{c} i_s \int \frac{\vec{t}' dl' dz'}{\sqrt{(\vec{\rho} - \vec{\rho}')^2 + (z - z')^2}}. \tag{A1}$$

The component of the magnetic field strength in the direction normal to the layer is

$$H_z' = -\frac{1}{c} i_s \int \frac{[(\vec{\rho} - \vec{\rho}') \times \vec{t}'] \vec{e}_z dl' dz'}{|\vec{r} - \vec{r}'|^3}. \tag{A2}$$

For the magnetic field strength averaged across the film we have

$$\langle H_z' \rangle = \frac{2 i_s}{cd} \int \frac{[(\vec{\rho} - \vec{\rho}') \times \vec{t}'] \vec{e}_z dl'}{|\vec{\rho} - \vec{\rho}'|} \Phi' \left(\frac{|\vec{\rho} - \vec{\rho}'|}{d} \right). \tag{A3}$$

Here $\Phi(\xi) = \ln(1/\xi + \sqrt{1 + 1/\xi^2}) + \xi - \sqrt{1 + \xi^2}$ and $\Phi'(\xi) = 1 - \sqrt{1 + 1/\xi^2}$.

The kinetic law for the interface motion (21) can be transformed as follows. The mean accross the film magnetic field $\langle \tilde{H}_z' \rangle$ is expressed as

$$\langle \tilde{H}'_z \rangle = \frac{1}{d}\int \frac{\partial \psi}{\partial z} dz = \frac{2\psi_+}{d} = -\frac{2M}{d}\int dS' J(\vec{\rho}-\vec{\rho}',d).$$

On the interface the following relation according to (7) is valid:

$$\langle \tilde{H}_z \rangle = -\frac{1}{2}H_n + \langle H'_z \rangle$$

where $\langle H'_z \rangle$ is found according to relation (A3) where the principal Cauchy value of the integral should be taken. Thus the law of the interface motion can be transformed as follows:

$$\begin{aligned} v_n &= -\frac{1}{\zeta}\left(\frac{H_c^2}{8\pi} + \sigma k - M\langle H'_z \rangle\right) \\ &= -\frac{1}{\zeta}\left(\frac{H_c^2}{8\pi} + \sigma k - \frac{H_n^2}{8\pi}\frac{1}{\pi d} \times \int \frac{[(\vec{\rho}-\vec{\rho}')\times \vec{t}']\vec{e}_z dl'}{|\vec{\rho}-\vec{\rho}'|}\Phi'\left(\frac{|\vec{\rho}-\vec{\rho}'|}{d}\right)\right). \end{aligned} \quad \text{(A4)}$$

The law of interface motion (A4) has a simple physical interpretation for the long cylindrical tube. In this case the Lorentz force per unit surface acting on the superconducting currents around the domain of the normal phase is $i_s/2cH_n\vec{n} = (H_n^2/8\pi)\vec{n}$. If the surface tension of the interface is neglected the interface motion according to the law $v_n = -1/\zeta(H_c^2/8\pi - H_n^2/8\pi)$ stops at $H_n = H_c$ as it should.

APPENDIX B

Applying the Evald summation technique the effective demagnetizing field coefficient is expressed as follows:

$$\begin{aligned} N_{dm}(x,y) = {} & \frac{\pi y^2}{2\sqrt{3}}\left[1 + \frac{4y}{3\pi x}\left(1 - \frac{(2k^2-1)E(k)}{k^3} - \frac{(1-k^2)K(k)}{k^3}\right)\right] + \frac{xy^4}{32\sqrt{3}}\left(\frac{8}{\pi x^2}\sum_{n_1,n_2\neq 0}\int_{|\vec{r}|\leq 1} d\vec{r}\, f(r)\left(\frac{1}{|y\vec{r}+\vec{\rho}_n|}\mathrm{erfc}(|y\vec{r}+\vec{\rho}_n|/\sqrt{\tau})\right.\right. \\ & \left. - \frac{1}{\sqrt{(y\vec{r}+\vec{\rho}_n)^2+x^2}}\mathrm{erfc}[\sqrt{(y\vec{r}+\vec{\rho}_n)^2+x^2}/\sqrt{\tau}]\right) - \frac{16}{x^2}\int_0^1 dr\, rf(r)\left[\frac{1}{yr}\mathrm{erf}\left(\frac{yr}{\sqrt{\tau}}\right) - \frac{1}{\sqrt{y^2r^2+x^2}}\mathrm{erf}\left(\frac{\sqrt{y^2r^2+x^2}}{\sqrt{\tau}}\right)\right] \\ & + \frac{8\pi^2}{\sqrt{3}x^2}\left\{x\ \mathrm{erf}\left(\frac{x}{\sqrt{\tau}}\right) - \sqrt{\frac{\tau}{\pi}}\left[1 - \exp\left(-\frac{x^2}{\tau}\right)\right]\right\} + \frac{8\pi^2}{\sqrt{3}x^2y^2}\sum_{n_1,n_2\neq 0}\frac{J_1^2(k_n y)}{k_n^3}\left[2\ \mathrm{erfc}(k_n\sqrt{\tau}) - \exp(2xk_n)\mathrm{erfc}\left(k_n\sqrt{\tau} + \frac{x}{\sqrt{\tau}}\right)\right. \\ & \left. + \exp(-2xk_n)\mathrm{erfc}\left(k_n\sqrt{\tau} - \frac{x}{\sqrt{\tau}}\right)\right]. \end{aligned} \quad \text{(B1)}$$

Here $k_n = 2\pi\sqrt{n_1^2+n_2^2-n_1n_2}/\sqrt{3}, n_i$ are natural numbers, $f(r) = 2(\arccos r - r\sqrt{1-r^2}), \vec{\rho}_n = n_1\vec{e}_1 + n_2\vec{e}_2$. τ in relation (23) is the Evald number for which the value 0.6 is taken in numerical calculations.

ACKNOWLEDGMENTS

This work was partially carried out during the stay of one of the authors (A.C.) at University P. M. Curie Paris 6. He is thankful for this opportunity. T.O. acknowledges financial support from the Leading Student Exchange Support Program and the Japanese Consortium of "College Doctoral franco-japonais."

*Electronic address: catherine.gourdon@insp.jussieu.fr; URL: http://www.insp.upmc.fr

[1] H. M. McConnell, Annu. Rev. Phys. Chem. **42**, 171 (1991).
[2] K. J. Stine, Ch. M. Knobler, and R. C. Desai, Phys. Rev. Lett. **65**, 1004 (1990).
[3] A. Cebers, M. M. Maiorov, Magn. Gidrodin. **16**, 27 (1980) [Magnetohydrodynamics (N.Y.) **16**, 21 (1980)].
[4] A. O. Cebers and M. M. Maiorov, Magnetohydrodynamics (N.Y.) **16**, 231 (1980).
[5] F. Elias, C. Flament, J-C. Bacri, and S. Neveu, J. Phys. I **7**, 711 (1997).
[6] R. E. Rosensweig, *Ferrohydrodynamics* (Dover Publications, Mineola, NY, 1997).
[7] S. A. Langer, R. E. Goldstein, and D. P. Jackson, Phys. Rev. A **46**, 4894 (1992).
[8] J. Richardi, D. Ingert, and M. P. Pileni, J. Phys. Chem. B **106**, 1521 (2002).
[9] M. Seul and R. Wolfe, Phys. Rev. A **46**, 7519 (1992).
[10] A. Hubert and R. Schäfer, *Magnetic Domains* (Springer, Berlin, 2000).

[11] T. E. Faber, Proc. R. Soc. London, Ser. A **248**, 460 (1958).
[12] F. Haenssler and L. Rinderer, Helv. Phys. Acta **40**, 659 (1967).
[13] R. P. Huebener, *Magnetic Flux Structures in Superconductors* (Springer, New York, 1979).
[14] R. Plass, N. C. Bartelt, and G. L. Kellogg, J. Phys.: Condens. Matter **14**, 4227 (2002).
[15] J. D. Murray, *Mathematical Biology*, 2nd corr. ed. (Springer, Berlin, 1993).
[16] R. E. Goldstein, D. J. Muraki, and D. M. Petrich, Phys. Rev. E **53**, 3933 (1996).
[17] M. Seul and D. Andelman, Science **267**, 476 (1995).
[18] S. A. Langer, R. E. Goldstein, and D. P. Jackson, Phys. Rev. A **46**, 4894 (1992).
[19] R. E. Goldstein, D. P. Jackson, and A. T. Dorsey, Phys. Rev. Lett. **76**, 3818 (1996).
[20] L. D. Landau, Zh. Eksp. Teor. Fiz. **7**, 371 (1937).
[21] R. E. Miller and G. D. Cody, Phys. Rev. **173**, 494 (1968).
[22] D. E. Farrell, R. P. Huebener, and R. T. Kampwirth, J. Low Temp. Phys. **19**, 99 (1975).
[23] R. N. Goren and M. Tinkham, J. Low Temp. Phys. **5**, 465 (1971).
[24] R. P. Huebener, R. T. Kampwirth, and V. A. Rowe, Cryogenics **12**, 100 (1972).
[25] R. P. Huebener and R. T. Kampwirth, Phys. Status Solidi A **13**, 255 (1972).
[26] A. T. Dorsey and R. E. Goldstein, Phys. Rev. B **57**, 3058 (1998).
[27] P. G. de Gennes, *Superconductivity of Metals and Alloys* (W.A. Benjamin, New York, 1966).
[28] C. R. Reisin and S. G. Lipson, Phys. Rev. B **61**, 4251 (2000).
[29] V. Jeudy, C. Gourdon, and T. Okada, Phys. Rev. Lett. **92**, 147001 (2004).
[30] D. E. Chimenti and J. R. Clem, Philos. Mag. B **38**, 635 (1978).
[31] V. Jeudy, G. Jung, D. Limagne, and G. Waysand, Physica C **225**, 331 (1994).
[32] H. Castro, B. Dutoit, A. Jacquier, M. Baharami, and L. Rinderer, Phys. Rev. B **59**, 596 (1999).
[33] L. Landau and E. Lifschitz, *Electrodynamics of Continous Media* (Nauka, Moscow, 1956).
[34] O. Narayan, Phys. Rev. Lett. **81**, 5035 (1998).
[35] R. E. Goldstein and A. T. Dorsey, Phys. Rev. Lett. **81**, 5036 (1998).
[36] H. Bokil and O. Narayan, Phys. Rev. B **56**, 11195 (1997).
[37] A. Cebers, Magn. Gidrodin. **30**, 179 (1994) [Magnetohydrodynamics (N.Y.) **30**, 148 (1994)].
[38] A. Cebers, Magn. Gidrodin. **31**, 61 (1995) [Magnetohydrodynamics (N.Y.) **31**, 58 (1995)].
[39] A. Cebers, Magn. Gidrodin. **26**, 49 (1990) [Magnetohydrodynamics (N.Y.) **26**, 309 (1990)].
[40] A. Hubert, Phys. Status Solidi **24**, 669 (1967).
[41] Yu. V. Sharvin, Zh. Eksp. Teor. Fiz. **38**, 298 (1960) [Sov. Phys. JETP **11**, 216 (1960)].
[42] G. Gourdon, V. Jeudy, M. Menant, D. Roditchev, Le Anh Tu, E. L. Ivchenko, and G. Karczewski, Appl. Phys. Lett. **82**, 230 (2003).
[43] C. Gourdon, G. Lazard, V. Jeudy, C. Testelin, E. L. Ivchenko, and G. Karczewski, Solid State Commun. **123**, 299 (2002).
[44] V. Jeudy, C. Gourdon, and A. Cebers (unpublished).
[45] For Hg we take $\Delta(0)$ equal to 0.084 μm, i.e., three times smaller than the value proposed in Ref. 22. The overestimation of $\Delta(0)$ in Ref. 22 results from the use of an approximate model to calculate the magnetic energy.
[46] W. H. Fietz, J. Parisi, and R. P. Huebener, J. Low Temp. Phys. **54**, 159 (1984).